



Perylene imide derivatives: Structural modification of imide position, aggregation caused quenching mechanism, light-conversion quality and photostability

Yuru Hu^{a,1}, Kai Wang^{b,1}, Yongtao Wang^{a,*}, Lei Ma^{b,**}

^a Guangxi Key Laboratory of Electrochemical and Magneto-chemical Function Material, College of Chemistry and Bioengineering, Guilin University of Technology, Guilin, 541004, PR China

^b Tianjin International Center for Nanoparticles and Nanosystem, Tianjin University, Tianjin, 300072, PR China

ARTICLE INFO

Keywords:

Light conversion agent
Photostability
Light conversion film
PDI derivatives
Light-conversion quality

ABSTRACT

To explore highly efficient yellow-green light conversion agents and the intrinsic mechanism of aggregation caused quenching of perylene imide derivatives, three perylene imide derivatives named as PDI-1, PDI-2 and PDI-3 were designed and synthesized, and their polyvinyl chloride, polybutylene adipate-polybutylene terephthalate (PBAT) copolymer and different ethylene-vinyl alcohol copolymers doping films were prepared. The perylene imide derivatives present similar solvatochromism in various solvents and fluorescence quenching in aggregated state, and then the intrinsic mechanism of fluorescence quenching was investigated by viscosity experiment, theoretical calculation and crystal analysis. Subsequently, light conversion quality of different doping films was measured and evaluated by using a HiPoint HR-450 analyzer in the range of 380–780 nm. Finally, photostability of the doping films was investigated by intensified ultraviolet light radiation (40 W). The results show that fluorescence quenching of the perylene imide derivatives has nothing to do with π - π stacking, which are attributed to twisted intramolecular charge transfer (PDI-2) and rotation and vibration of molecular bonds (PDI-1 and PDI-3). After UV radiation of 30 h, emission intensities of 25%EVA@film and 40%EVA@film fluctuate only slightly. From this, a simple and efficient way to enhance photostability was obtained by choosing amphiphilic EVA copolymers.

1. Introduction

The absorption spectra of pigments in leaves shows that the yellow-green light (510–580 nm) in sunlight cannot be absorbed by crops [1,2]. By adding light conversion materials to the greenhouse film, yellow-green light is converted into red-orange light (600–700 nm) required for crop photosynthesis, which can increase crop yield, shorten growth cycle, and improve nutrients efficiently [3–5]. However, the current research on light conversion agents mainly focuses on the conversion of ultraviolet light, while the exploitation of yellow-green light conversion agents is relatively lagging [6–8].

Currently, some yellow-green light conversion agents including inorganic rare earth oxides, diketopyrrolopyrrole and perylene bisimide (PDI) derivatives have been reported [9]. Among of them, inorganic rare earth oxides have higher preparation conditions. the preparation

process requires high-temperature calcination, grinding and high-purity rare earth materials, and the particle size is closely related to the light conversion performance [10–12]. Compared with inorganic rare earth oxides, diketopyrrolopyrrole (DPP) and perylene bisimide (PDI) derivatives have good resin compatibility, tunable emission wavelengths, and recyclable raw materials [13–17]. Especially, some DPP and PDI derivatives present aggregation induced emission (AIE) activity, which can reduce the fluorescence quenching caused by uneven doping and enhance light conversion efficiency. Furthermore, DPP and PDI derivatives have the potential to be used as yellow-green light conversion agent [17,18].

Recently, Tang et al. [19] obtained AIE-active PDI derivatives by introducing propeller-like tetraphenylethylene (TPE) units at bay-position of PDI core. Li et al. [20] also designed and synthesized a series of PDI derivatives by chemical modification of bay-position, but the re-

* Corresponding author.

** Corresponding author.

E-mail addresses: wyt_shzu@163.com (Y. Wang), lei.ma@tju.edu.cn (L. Ma).

¹ Yuru Hu and Kai Wang contributed equally.

<https://doi.org/10.1016/j.dyepig.2022.110948>

Received 12 September 2022; Received in revised form 10 November 2022; Accepted 15 November 2022
0143-7208/© 20XX

sults found that only PDI derivatives with large steric hindrance showed AIE activity. Hwang et al. [21] prepared some DPP derivatives, and their AIE activity and light conversion properties were further confirmed and investigated. However, synthesis of the AIE-active PDI and DPP derivatives is complex on the one hand, and fluorescence quantum yields of the AIE-active dyes in doping films are significantly lower than that of PDI derivatives with aggregation caused quenching (ACQ) activity on the other hand, which was previously reported in our laboratory. Therefore, it is desirable to integrate easy preparation, AIE-activity and high fluorescence quantum yields into light conversion agents. More importantly, organic fluorescent dyes are easy to be bleached and degraded under solar radiation, but efficient means to enhance photostability are still lacking. Based on theoretical calculation, some ACQ-active PDI derivatives present twist molecular configuration, which is not conducive to intermolecular π - π stacking, but their ACQ mechanism is often simply attributed to intermolecular π - π stacking. To solve the above problem, three PDI derivatives were designed and synthesized by tuning steric resistance effect of imide positions (Fig. 1), and the corresponding optical properties were investigated and discussed in detail based on UV-Vis absorption and fluorescence emission spectra, AIE-activity, light conversion quality, photostability, crystal analysis and theoretical calculation.

2. Experimental details

2.1. Measurements and characterizations

^1H NMR spectra and ^{13}C NMR spectra were obtained by Varianova instrument at 500MHz and 100MHz, respectively, using CDCl_3 and $\text{DMSO}-d_6$ as solvents and tetramethylsilane (TMS) as internal standard. UV-vis absorption spectra were recorded from 200 to 800 nm on a MaPada UV-3200PCS spectrophotometer using a 1.0 cm quartz cell. The fluorescence emission spectra were measured on a Hitachi F-2500 fluorescence spectrophotometer using a 150 W xenon arc lamp as the light source. Emission spectra were recorded within wavelength range of 550 nm–800 nm, and the photomultiplier tube voltage was 700 V. Both excitation and emission slits were set at 5.0 nm, and no filter was used. 1×1 cm four-sided transparent quartz cuvette was applied as a sample cell, and corrections of spectral profiles regarding the excitation source and detector were conducted by distilled water and printing paper. MALDI/HRMS was recorded on UltrafleXtreme MALDI-TOF/TOF mass spectrometer (Bruker, Germany). Light conversion

quality of the doping films was measured and evaluated by using a Hi-Point HR-450 analyzer in the range of 380–780 nm.

2.2. Materials and synthesis

The intermediary named 2a and its respective derivative PDI-1 were obtained (Fig. 1) according to the synthesis method reported in the literature [22,23]. The chemicals and reagents used in this study are of analytical grade and do not need further purification. All intermediates and final compounds were purified by silica gel (200–300 mesh) column chromatography, and the reaction was monitored by TLC.

Synthesis of 5,6,12,13-tetrachloro-2,9-bis(2,6-diisopropylphenyl) anthra[2,1,9-def:6,5,10-d'e'f]diisoquinoline-1,3,8,10(2H,9H)-tetraone (2a): 1,6,7,12-tetrachloroperylene-3,4,9,10-tetracarboxylic dianhydride (0.8 g, 1.5 mmol) and 2,6-diisopropylaniline (1.13 ml, 6.0 mmol) were dissolved in 30 mL propionic acid and refluxed at 130 °C in argon atmosphere for 16 h. After cooling to room temperature, the reaction mixture was poured into 500 mL of water, filtered and collected the precipitate, and washed with water until the pH was neutral. The crude product was purified by chromatography (silica gel, CH_2Cl_2 /petroleum ether, v/v = 1:3), and orange solid was obtained. Yield: 80%.

Synthesis of 2,9-bis(2,6-diisopropylphenyl)-5,6,12,13-tetraphenoxyanthra[2,1,9-def:6,5,10-d'e'f]diisoquinoline-1,3,8,10(2H,9H)-tetraone (PDI-1): Compound 2a (0.85 g, 1 mmol), phenol (0.8 mL, 8 mmol) and anhydrous K_2CO_3 (0.55 g, 4 mmol) were dissolved in anhydrous NMP (30 ml), kept at 90 °C under argon protection, heated and refluxed for 12h. After cooling to room temperature, the reaction solution was poured into water and extracted with ethyl acetate. The obtained organic layer was dried with anhydrous Na_2SO_4 and evaporated in vacuum. The crude product was purified by silica gel column chromatography (silica gel, ethyl acetate: petroleum ether = 1:10). A red solid was obtained. Yield: 90%. ^1H NMR (500 MHz, CDCl_3) δ 8.27 (s, 4H), 7.45–7.42 (t, J = 15.0 Hz, 2H), 7.28 (d, J = 10.0 Hz, 6H), 7.26 (s, 6H), 7.12–7.09 (t, J = 15.0 Hz, 4H), 6.98 (d, J = 10.0 Hz, 8H), 2.73–2.68 (m, 4H), 1.12 (d, J = 5.0 Hz, 24H) (Fig. S1). HRMS (MALDI-TOF): m/z 1101.4085 $[[\text{M} + \text{H}]^+]$, calculated 1101.4080 (Fig. S2).

Synthesis of 4-(1,2,2-triphenylvinyl)anilin: Bromotriphenylethylene (1.12 g, 3.3 mmol) and 4-aminophenylboronic acid (0.55 g, 4 mmol) were mixed in THF (50 mL) in a 250 mL round-bottom flask, mixed and degassed in the presence of 2 mol/L K_2CO_3 solution (3 mL) and TBAB (3.3 mg, 0.01 mmol), and stirred for 30 min under argon protection. Then, catalyst $\text{Pd}(\text{PPh}_3)_4$ (0.19 g, 0.165 mmol) was added and kept at

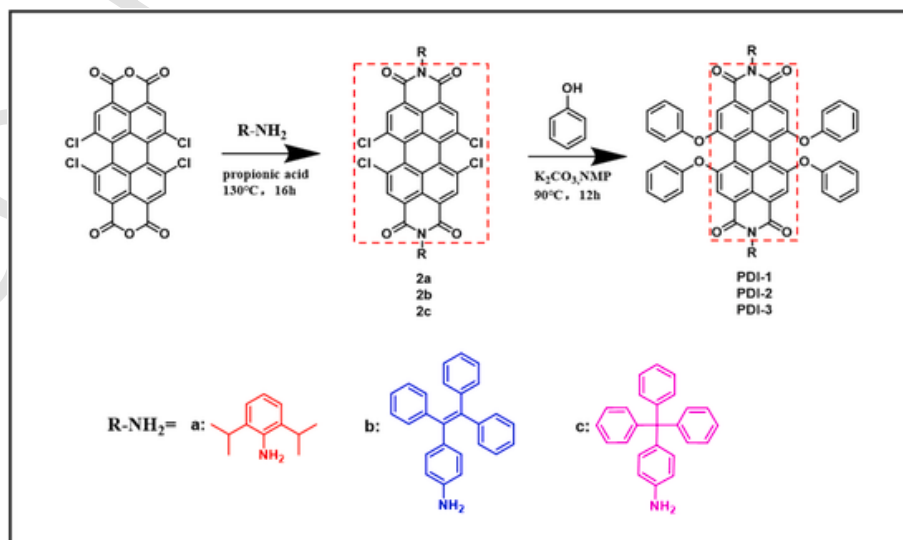


Fig. 1. Synthetic routes of PDI-1, PDI-2, PDI-3.

80 °C for 24 h. After cooling to room temperature, the reaction solution was poured into water and extracted with dichloromethane. The obtained organic layer was dried with anhydrous Na₂SO₄ and evaporated in vacuum. The crude product was purified by silica gel column chromatography (silica gel, CH₂Cl₂: petroleum ether, v/v = 1:2) to obtain a light-yellow solid. Yield: 89%.

Synthesis of 5,6,12,13-tetrachloro-2,9-bis(4-(1,2,2-triphenylvinyl)phenyl)anthra[2,1,9-def:6,5,10-d'e'f]diisoquinoline-1,3,8,10(2H,9H)-tetraone (2b): 1,6,7,12-tetrachloroperylene-3,4,9,10-tetracarboxylic dianhydride (0.1 g, 0.19 mol) and 4-(1,2,2-triphenylvinyl) aniline (0.28 g, 0.8 mmol) were mixed in acetic acid (3 mL) and anhydrous NMP (10 mL), kept the temperature at 120 °C under the protection of argon, and refluxed for 12h. After cooling to room temperature, the reaction solution was poured into 10% hydrochloric acid solution, filtered and collected the precipitate, and washed with water until the pH was neutral. The crude product was purified by chromatography (silica gel, CH₂Cl₂/petroleum ether, v/v = 1:1) to obtain orange solid. Yield: 78%.

Synthesis of 5,6,12,13-tetraphenoxy-2,9-bis(4-(1,2,2-triphenylvinyl)phenyl)anthra[2,1,9-def: 6,5,10-d'e'f]diisoquinoline-1,3,8,10(2H,9H)-tetraone (PDI-2): Compound 2b (1.19 g, 1 mmol), phenol (0.8 mL, 8 mmol) and anhydrous K₂CO₃ (0.55 g, 4 mmol) were dissolved in anhydrous NMP (30 mL), kept at 90 °C under argon protection, heated and refluxed for 12h. After cooling to room temperature, the reaction solution was poured into 10% hydrochloric acid solution, filtered and collected the precipitate, and washed with water until the pH was neutral. The crude product was purified by silica gel column chromatography (silica gel, CH₂Cl₂/petroleum ether, v/v = 1:1) to obtain a red solid. Yield: 82%. ¹H NMR (500 MHz, DMSO-*d*₆) δ 8.41 (s, 1 H), 7.90–7.81 (m, 3H), 7.54 (t, *J* = 10.0Hz, 2H), 7.34–6.99 (m, 56 H) (Fig. S3). ¹³C NMR (100 MHz, CDCl₃) δ 163.38, 156.06, 155.18, 143.61, 143.37, 143.31, 141.68, 133.08, 132.13, 131.48, 131.36, 130.04, 127.80, 127.72, 127.68, 126.83, 126.55, 124.75, 122.75, 120.66, 120.34, 120.09, 119.81 (Fig. S4). HRMS (MALDI-TOF): *m/z* 1419.4579 [[M+H]⁺, calculated 1419.4574] (Fig. S5).

Synthesis of 5,6,12,13-tetrachloro-2,9-bis(4-tritylphenyl)anthra[2,1,9-def:6,5,10-d'e'f] diiso quinoline-1,3,8,10(2H,9H)-tetraone (2c): Using 1,6,7,12-tetrachloroperylene-3,4,9,10-tetracarboxylic dianhydride and 4-triphenylmethylaniline, the compound was synthesized by the same procedure as described for the intermediate 2a. The crude product was purified by chromatography (silica gel, CH₂Cl₂/petroleum ether, v/v = 1:1) to obtain orange solid. Yield: 80%.

Synthesis of 5,6,12,13-tetraphenoxy-2,9-bis(4-tritylphenyl)anthra[2,1,9-def:6,5,10-d'e'f]diiso quinoline-1,3,8,10(2H,9H)-tetraone (PDI-3): Using compound 2c and phenol, this compound was synthesized by the same procedure as described for PDI-1. The crude product was purified by chromatography (silica gel, ethyl acetate/petroleum ether, v/v = 1:5) to obtain a red solid. Yield: 83%. ¹H NMR (500 MHz, DMSO-*d*₆) δ 8.45 (s, 1 H), 7.95–7.88 (t, *J* = 35.0Hz, 3H), 7.53–7.01 (m, 58 H) (Fig. S6). ¹³C NMR (100 MHz, CDCl₃) δ 163.51, 163.05, 156.12, 155.18, 153.94, 147.51, 147.39, 146.45, 135.08, 133.11, 132.59, 132.09, 132.00, 131.19, 130.40, 130.13, 130.04, 129.61, 127.61, 127.46, 126.10, 125.64, 125.00, 124.79, 124.07, 122.73, 121.19, 120.73, 120.57, 120.32, 120.08, 119.86, 115.50, 64.88, 31.47, 30.23, 29.73 (Fig. S7). HRMS (MALDI-TOF): *m/z* 1417.4409 [[M+H]⁺, calculated 1417.4410] (Fig. S8).

2.3. Preparation of light conversion films

polyvinyl chloride (PVC)/polybutylene adipate-polybutylene terephthalate copolymer (PBAT)/25% ethylene-vinyl alcohol copolymers (EVA)/40% EVA (1 g) and PDI-1 (0.01 g) were dissolved into 15 mL THF in a single-necked flask, placed in ultrasonic oscillator for 3h, and mixed evenly. Poured the mixture on a glass plate and spread it quickly with a glass rod. Finally, the films were put into a ventilated

cabinet until the THF was volatilized completely, and the corresponding light conversion film of PDI-1 (1% mass fraction) including 1%PVC@film, 1%/10%PBAT@film, 25%EVA@film and 40%EVA@film were obtained. According to this method and previously reported documents [24,25], other light conversion films were obtained.

3. Results and discussion

3.1. Solvatochromism

To observe different substitution effects of imide positions, the UV-Vis absorption and fluorescence emission spectra of 2a, 2b, 2c and their PDI derivatives were investigated in various solvents (10 μmol/L). As shown in Fig. 2, the three compounds have similar absorption and emission curves, indicating that the electron-donating substituents at the imide positions have unobvious interference on the photophysical properties of PDI chromophore. As speculation, the radiation transitions of the three molecules all occur between the frontier orbitals of PDI nuclei. Furthermore, the absorption spectra present three different absorption bands around 440 nm, 530 nm and 570 nm, which correspond to S₀-S₂ (440 nm and 530 nm) and S₀-S₁ transition (570 nm) respectively [26]. Generally, absorption and emission maxima appear red shift with the increase of solvent polarity from Tol, DCM to DMSO, while abnormal blue-shift for THF may be due to interactions between solute and solvent. Compared with absorption maxima, emission maxima give more significant redshifts in various solvents, demonstrating larger dipole moment for excited state than ground state. In the same solvent, bathochromic shift of absorption and emission maxima can be observed in the order of PDI-3, PDI-2 and PDI-1 (Fig. 2 and Table S1), illustrating gradually enhanced electron-donating ability from tetraphenylmethane (TPM), tetraphenylethylene (TPE) to 2,6-diisopropyl benzene (DIPB). In n-hexane, absorption spectra of PDI-1 are similar to that of other solvents, while absorption spectra of PDI-2 and PDI-3 show obvious redshift and widening, which is due to poor solubility caused by TPM and TPE units, not only forming single molecule but also aggregated state. Worse still, fluorescence of PDI-3 was completely quenched in n-hexane due to aggregation. By contrast, the absorption and emission maxima of 2a, 2b and 2c relative to their PDI derivatives show obvious blue-shift (Fig. 2 and Fig. S10). For 2b, the energy of the excited state is rapidly exhausted due to intramolecular rotation and vibration induced by two TPE units in various solution, emitting extremely weak fluorescence in the dissolved state.

3.2. Aggregation-induced emission

Based on our previous research results, PDI-1 suffers from fluorescence quenching in solid state, which is attributed to π-π stacking induced by planar molecular skeleton of PDI [23]. If the above-mentioned conclusion is correct, assembling highly twisted TPE and TPM units should be able to relieve or even inhibit intermolecular π-π stacking, thereby AIE characteristics of three PDI derivatives were investigated by adopting THF and H₂O as benign solvents and non-benign solvents respectively. The reported literatures show that high water fraction (*f_w*) easily leads to red-shift of emission wavelength due to increased solvent polarity, while the formation of aggregated states often leads to blue-shift of emission wavelength. Under the combined action of solvent polarity and aggregation effect, emission wavelength of PDI-1 presents N-shaped fluctuations, but continuous red-shift for PDI-2 and PDI-3, except for slight blue-shift of PDI-3 at *f_w* = 90%. Quite unexpectedly, fluorescence intensity of PDI-1 and PDI-3 continue to decline with the increase of *f_w*, only PDI-2 with a tiny increase at *f_w* = 80–90%, outlining obvious ACQ characteristic (Fig. 3), what's more, PDI-2 shows the worst fluorescence emission in three PDI derivatives, whose fluorescence intensities are only 8%–10% that of PDI-1 and PDI-3 during AIE testing.

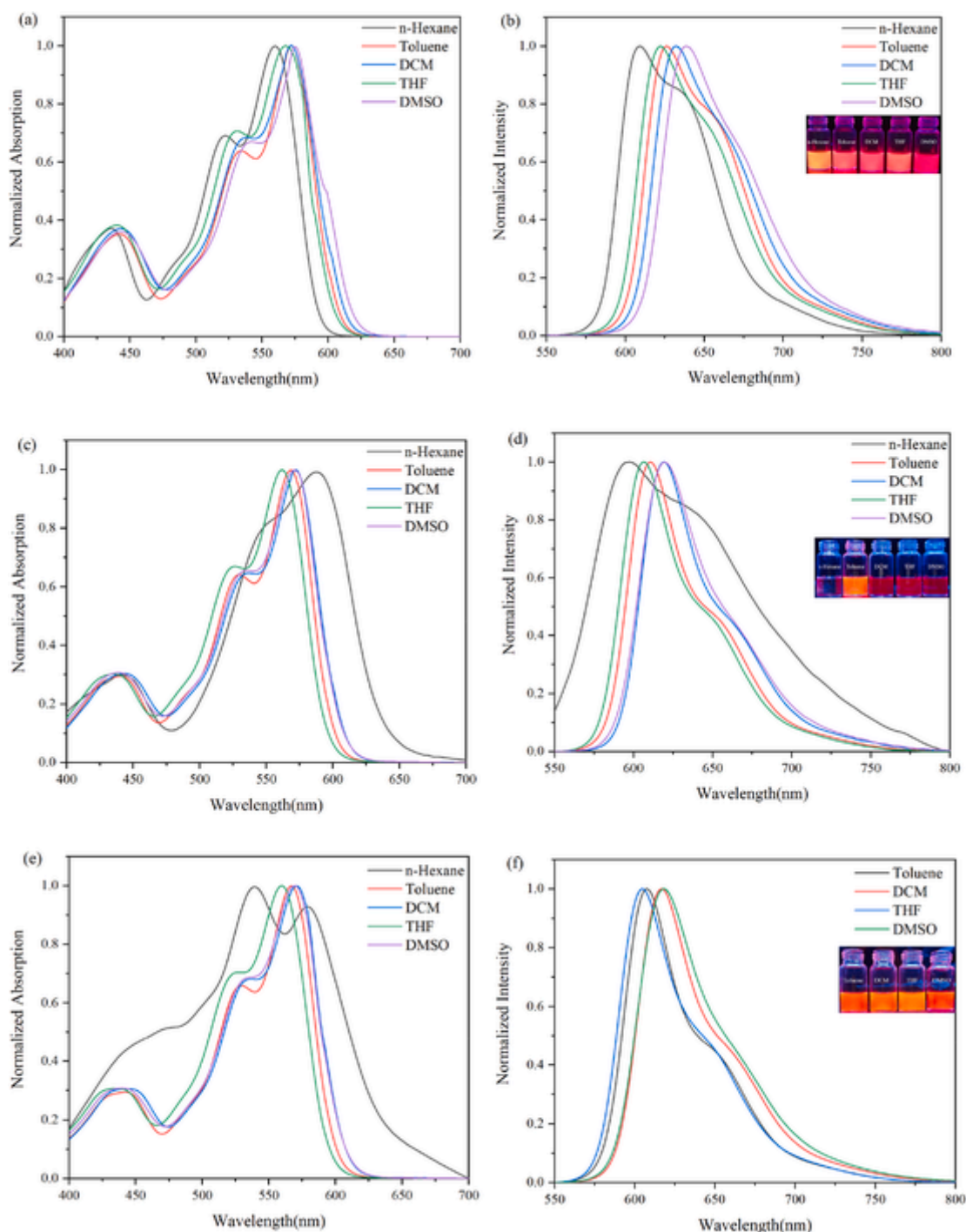


Fig. 2. Normalized UV-vis absorption spectra of (a) PDI-1, (c) PDI-2, (e) PDI-3 in various solvents. Normalized fluorescence spectra of (b) PDI-1, (d) PDI-2, (f) PDI-3 in various solvents. (Solution concentration: 10 $\mu\text{mol/L}$. Inset is the irradiation of different solvents under 365 nm UV illumination.).

What mechanism is responsible for ACQ effect of the PDI derivatives? Firstly, we speculated that the deteriorated fluorescence emission come from intramolecular rotation and vibration, especially for PDI-2 with TPE unit. Secondly, highly twisted TPE and TPM units still cannot suppress intermolecular π - π stacking, which lead to fluorescence quenching of aggregated state. Thirdly, DIPB, TPE and TPM units act as electron donors (D), while PDI core acts as electron acceptors (A), forming highly distorted D-A molecules. To verify the first conjecture, AIE characteristics of the PDI derivatives were investigated again by adjusting the viscosity of the solvents. With the increase of glycerol fraction, fluorescence emission of PDI-1, PDI-2 and PDI-3 become weaker and weaker (Fig. S9), and the situation is the same as the above THF-H₂O

system. On the one hand, the first conjecture may not be the main reason for fluorescence quenching. On the other hand, twisted molecular configuration of the PDI derivatives easily produce large voids, thereby viscosity of glycerol is still not enough to inhibit intramolecular and intermolecular rotation and vibration of C-C and C-N bonds. To explore the real reason of ACQ for the PDI dyes, subsequently, theoretical calculation and crystal analysis were carried out.

3.3. Crystal analysis and theoretical calculation (CCDC 2205299)

Suitable crystal for X-ray analyses were grown by slow diffusion of n-hexane into a solution of PDI-1, PDI-2 or PDI-3 in dichloromethane at

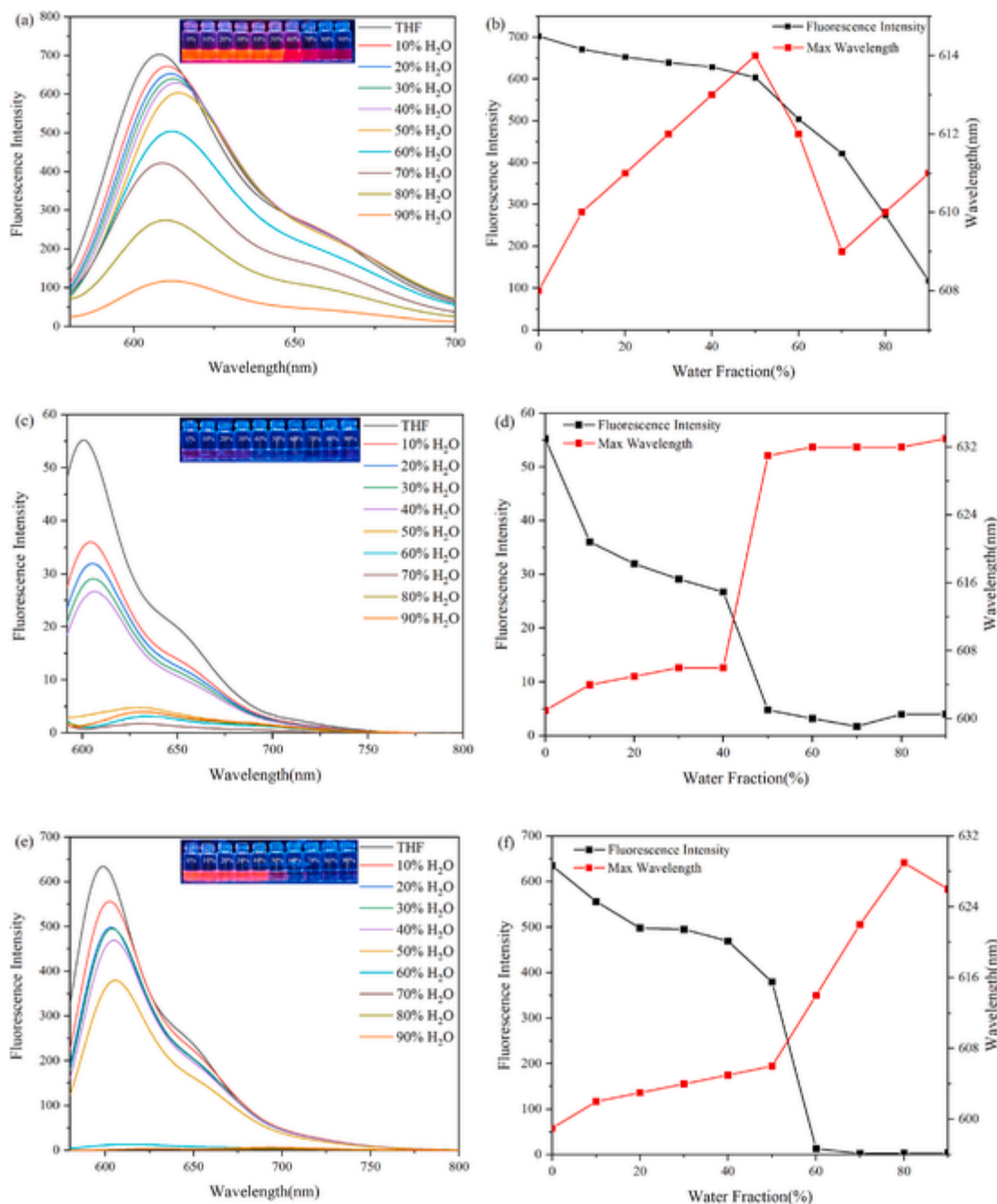


Fig. 3. Fluorescence emission spectra of (a) PDI-1, (c) PDI-2, (e) PDI-3 in THF/water mixtures with different water contents. Photos of the relationship between the fluorescence emission peak intensity/wavelength of (b) PDI-1, (d) PDI-2 and (f) PDI-3 and water fraction. (Solution concentration: 10 $\mu\text{mol/L}$. Inset: Photographs in THF/water mixtures with different fractions of water under 365 nm UV illumination).

room temperature. Fortunately, PDI-1 crystal was obtained after several days, and crystal structure, intermolecular arrangement, stacking and weak interactions of PDI-1 are investigated. PDI-1 (CCDC) belongs to monoclinic system with the space group of $C12/c1$, $a = 20.3287(13)$ Å, $b = 13.6627(12)$ Å, $c = 23.3614(19)$ Å, $\beta = 97.277(2)^\circ$. Fig. 4a shows two naphthalimide units of PDI core twist in the opposite direction around geometric center of molecule, and their dihedral angle is about 33.27° . Significantly, naphthalimide unit itself also presents a twisted molecular configuration, the corresponding dihedral angles between ring A-B, B-C and A-C are 8.47° , 4.39° and 6.82° . The diisopropyl benzene and the benzene ring on the bay position tend to approximate vertical conformation with PDI core, whose dihedral angles are 76.21° , 76.19° and 75.54° for ring C-D, A-E and B-F in turn. The unit cell contains six molecules, whose volume and density are $6436.2(9)$ Å³ and

1.114 g/cm^3 , respectively. Viewed from the b-axis direction, PDI-1 molecules are regularly arranged in a bricked fashion (Fig. 4b). Along the c-axis direction, the dimer forms J-type stacking with plane to plane (C_p-C_p) of 6.786 Å and centroid to centroid (C_g-C_g) of 6.873 Å distances (Fig. 4c). Along the a-axis, PDI-1 adopts parallel head-to-head stacking, forming C_p-C_p with 5.161 Å distances and C_g-C_g with 5.897 Å distances between adjacent intermolecular diisopropyl benzenes respectively (Fig. 4d). Obviously, the distorted molecular configuration and large C_p-C_p rule out the formation of $\pi-\pi$ stacking. Interestingly, the intermolecular weak interactions at both ends of PDI core presents perfectly symmetric, whose powerful $C-H\cdots C$ (2.845 , 2.893 Å), $C\cdots H$ (2.845 , 2.893 Å), $C-O\cdots H$ (2.704 , 2.648 Å) and $C-H\cdots C$ (2.893 Å) contribute to maintain the twisted molecular conformation (Fig. 4e). Subsequently, the structures of three PDI molecules were optimized at PBE0/

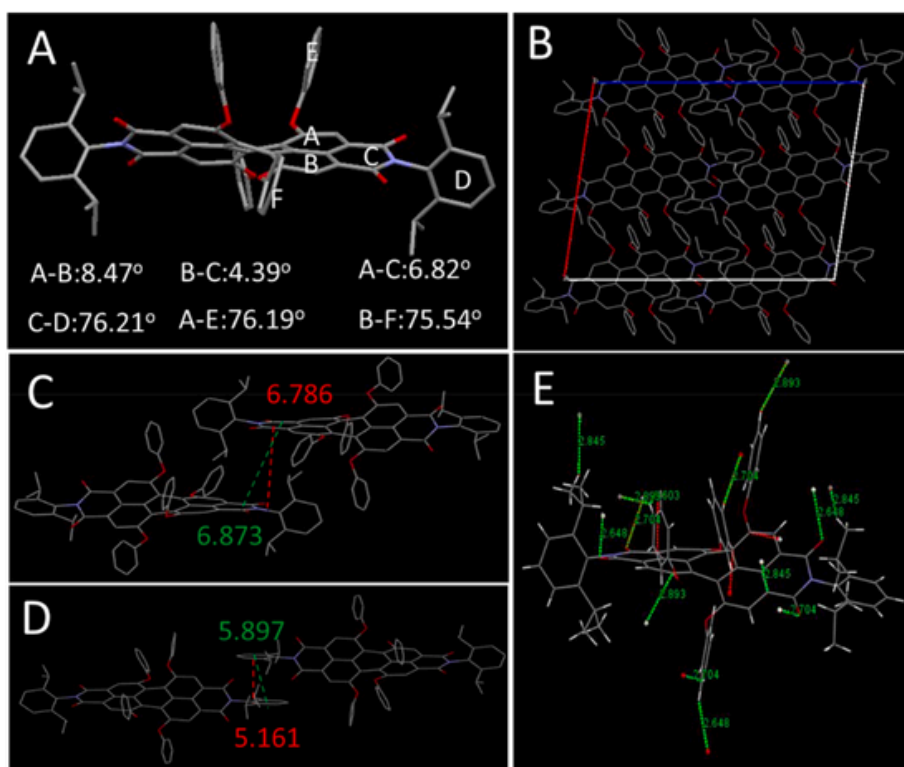


Fig. 4. Single crystal structure and conformation, unit cell and intermolecular stacking modes ignoring hydrogen atoms, and hydrogen bond and weak interaction sites for PDI-1.

def2-SVP level, and the def2-TZVP basis set was used in the calculations. All the density functional theory (DFT) calculations were performed on ORCA program [27]. The visualization of electron distribution was performed by using the Multiwfn 3.8 (dev) [28] and VMD 1.9.3 [29], respectively. As shown in Fig. 5, the highest occupied molecular orbital (HOMO) and lowest unoccupied molecular orbital (LUMO) are mainly concentrated on PDI core for PDI-1 and PDI-3, while HOMO and LUMO of PDI-2 are located on electron-donating TPE moiety and electron-withdrawing PDI core respectively, outlining obviously twisted intramolecular charge transfer (TICT) effect. We know that the large HOMO-LUMO overlap contributes to electron delocalization and enhancement of radiative transition rate, giving rise to strong fluorescence emission, but spatial separation of HOMO-LUMO generally leads to an opposite result, which should be responsible for inferior fluorescent emission of PDI-2 in both solid-state and solution. For PDI-1 and PDI-3, the key to enhance fluorescence emission may be to suppress intramolecular and intermolecular rotation and vibration of C-C, C-O and C-N bonds.

3.4. Light-conversion quality

By dissolving PDI-1/PDI-2/PDI-3 and PVC/PBAT/25% EVA (Polyvinyl alcohol accounts for 25% of the weight of EVA copolymer)/40% EVA (Polyvinyl alcohol accounts for 40% of the weight of EVA copolymer) at a weight ratio of 1:100, various doping films named as 1%PVC@film, 1%PBAT@film, 25%EVA@film and 40%EVA@film were prepared. when PDI-1/PDI-2/PDI-3 and PVC/PBAT were dissolved at a weight ratio of 1:10, the corresponding doping films were named as 10%PVC@film and 10%PBAT@film. The blank films without PDI dyes were used as the control, then light conversion quality of the doping films was measured and evaluated by using a Hi-Point HR-450 analyzer in the range of 380–780 nm. Taking PDI-1 as an example, Fig. 6a shows spectral intensity of the 1%PBAT@film decreases prominently compared with that of the blank film at 380–600 nm, especially for 500–600 nm, while intensity maxima and the photosynthetic photon flux density (PPFD) increased up to 85% and 65% compared with that of blank film at 600–700 nm, moreover, spectral composition of 600–700 nm sharply increases to 62% from 28%, which show

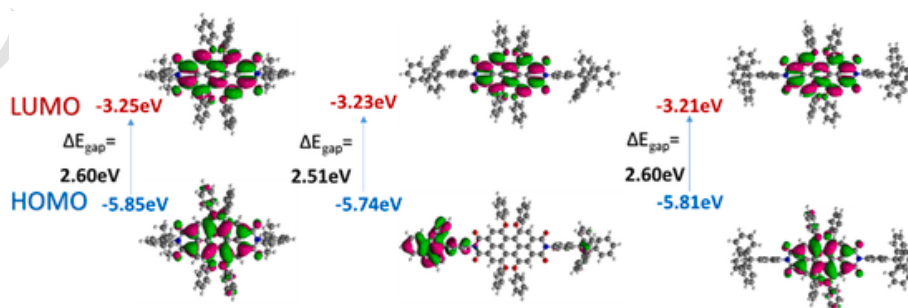


Fig. 5. B3LYP/6-31G (d, p) calculated molecular orbital amplitude plots of HOMO and LUMO levels for PDI-1.

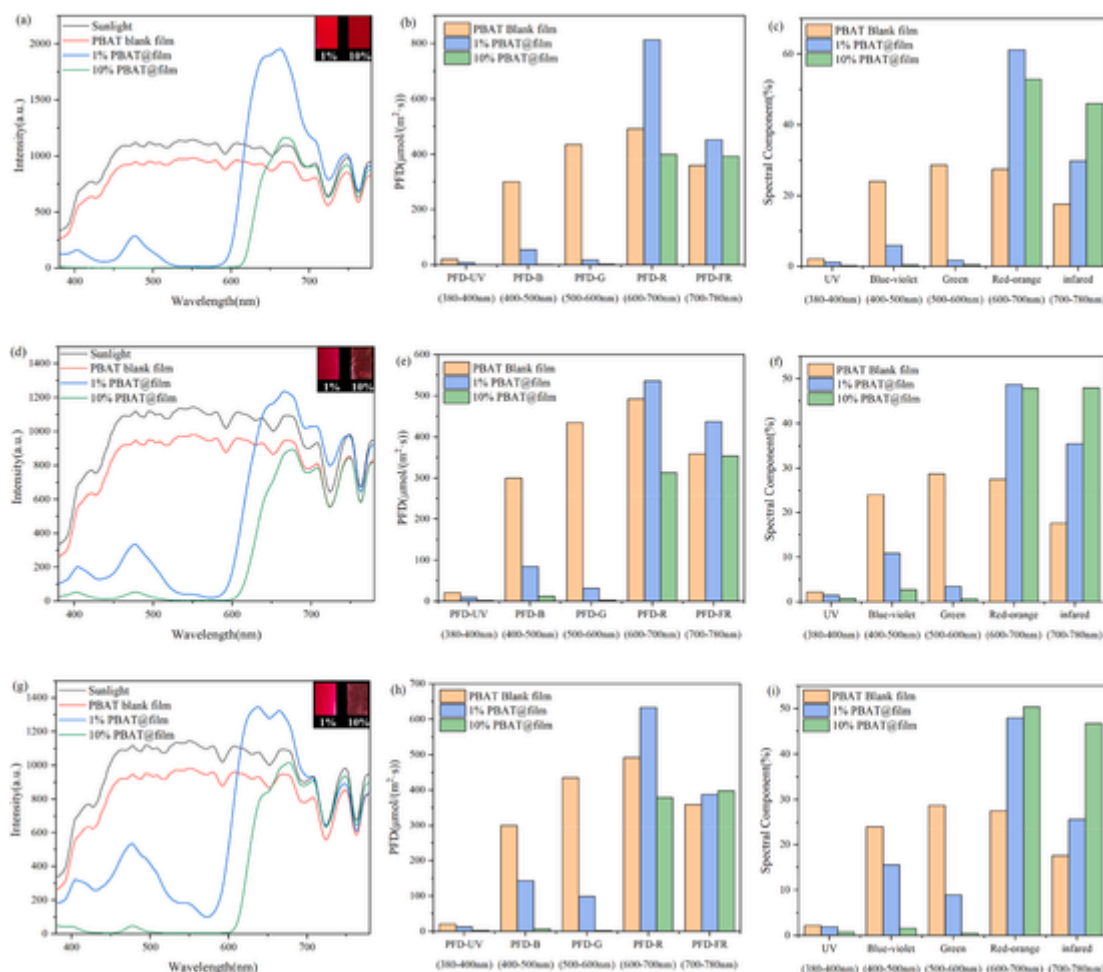


Fig. 6. Measure the light quality under the PBAT blank film and 1%/10%PBAT@film of (a) PDI-1, (d) PDI-2 and (g) PDI-3; PFD measured under sunlight in PBAT blank film and 1%/10%PBAT@film of (b) PDI-1, (e) PDI-2 and (h) PDI-3; Spectral components measured under sunlight in PBAT blank film and 1%/10%PBAT@film of (c) PDI-1, (f) PDI-2 and (i) PDI-3. (Inset: photographs of doped films taken in natural light.)

that the doping films have excellent yellow-green light conversion properties. By contrast, 1%PBAT@films of PDI-2 and PDI-3 also exhibit obviously yellow-green light conversion properties, however, according to PFD, spectral components and spectral intensity, light conversion quality deteriorated significantly, especially for PDI-2, which is attributed to TICT effect and poor compatibility between PDI-2 and PBAT. Compared with 1%PBAT@film, the spectral intensity of 10%PBAT@film at 600–700 nm decreased significantly (Fig. 6), meaning deteriorated light conversion performance with the increase of doping concentration. Considering the ACQ effect of the PDI compounds, it is reasonable that the high doping concentration easily leads to the decrease of light conversion efficiency. 1%PVC@film, 25%EVA@film and 40%EVA@film have similar light conversion performance to the corresponding 1%PBAT@film, but their spectral intensity and PFD decreased slightly (Fig. 6a–c, Fig. 7a–c and Fig. S12 a–e), which may be due to the relatively poor compatibility between the PDI derivatives with PVC/25%EVA/40%EVA. Compared with PBAT@film, 25%EVA@film and 40%EVA@film, spectral intensity between PVC blank film and sunlight is closer, illustrating better light transmission for PVC film than the other films. By covering the school emblem with 1%PBAT@film, 25%EVA@film and 40%EVA@film respectively, the texts below the films are clearly visible, revealing excellent light transmission (Fig. S14 a–c).

3.5. Photostability, high temperature and humidity stability

The photobleaching mechanisms of organic fluorescent dyes indicate that the majority of known photobleaching pathways involve reactive oxygen species [30–33], generated by reaction of triplet exciton with molecular oxygen. By reducing the oxygen content around chromophores, the corresponding photostability is expected to be greatly improved. Furthermore, polyvinyl alcohol is often used as a doping matrix to block the diffusion of oxygen by strong intermolecular hydrogen bonds. Inspired by this, EVA are chosen as doping matrix, where hydrophobic polyethylene facilitates the uniform dispersion of fluorescent dyes, while hydrophilic polyvinyl alcohol can inhibit oxygen diffusion. Then 25%EVA@film and 40%EVA@film are prepared by dissolving PDI-1 and 25%EVA/40%EVA at a weight ratio of 1:100. Photodegradation of the light-conversion agents is often accelerated in PVC film due to the release of hydrogen chloride. Therefore, for comparison, photodegradation of 1%PBAT@film, 25%EVA@film and 40%EVA@film was investigated by intensified ultraviolet light radiation (40 W). After UV radiation of 30 h, emission maxima of three PDI-1 do not show obvious shift in 1%PBAT@film, but fluorescence intensity gradually decreases with the increase of irradiation time. By contrast, emission intensity of 1%PBAT@film maintains 78.3% of the initial value, while 25%EVA@film and 40%EVA@film show excellent photostability, whose emission intensities fluctuate only slightly. In addition, light conversion materials need to withstand high temperature and humidity environment, therefore, photostability of 25%EVA@film and

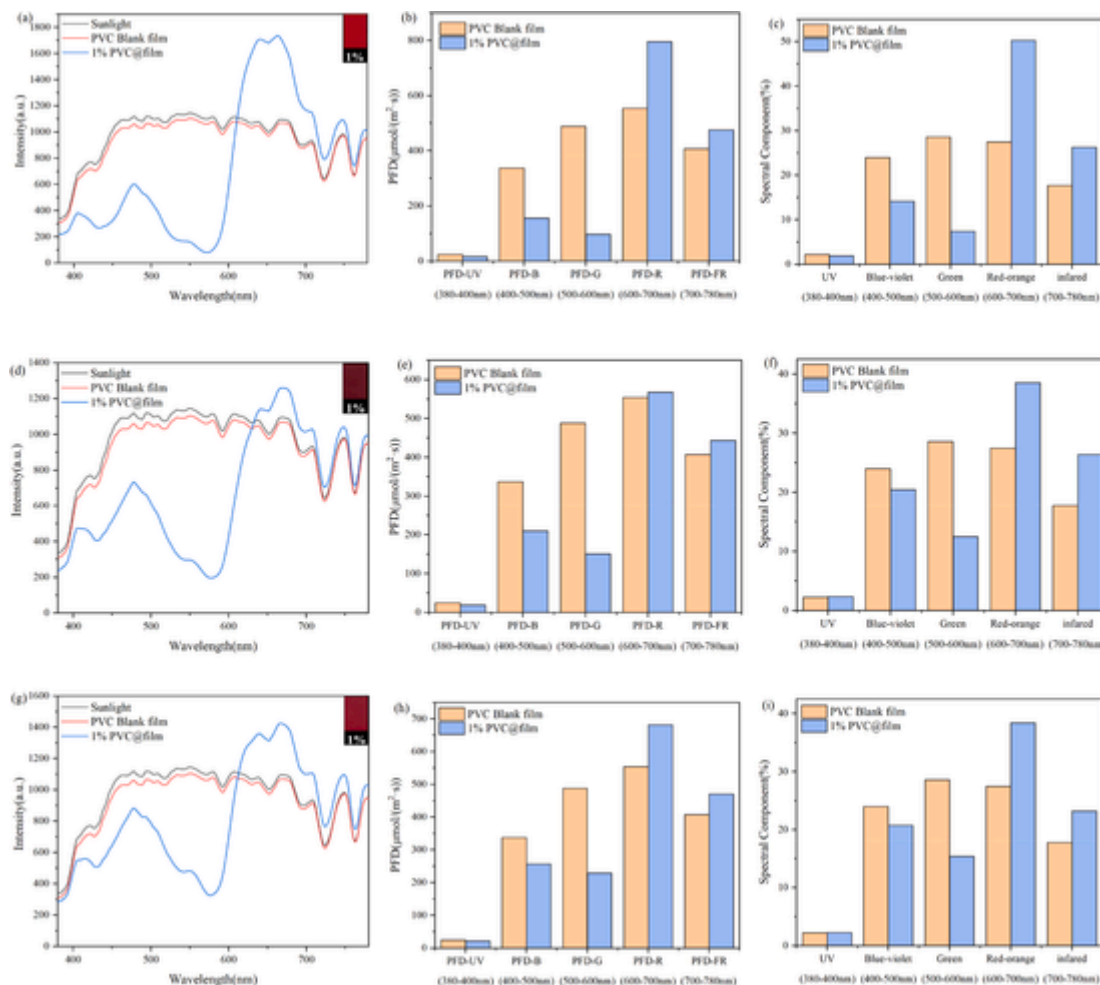


Fig. 7. Measure the light quality under the PVC blank film and 1%PVC@film of (a) PDI-1, (d) PDI-2 and (g)PDI-3; PFD measured under sunlight in PVC blank film and 1%PVC@film of (b) PDI-1, (e) PDI-2 and (h) PDI-3; Spectral components measured under sunlight in PVC blank film and 1%PVC@film of (c) PDI-1, (f) PDI-2 and (i) PDI-3. Inset: photographs of doped films taken in natural light.)

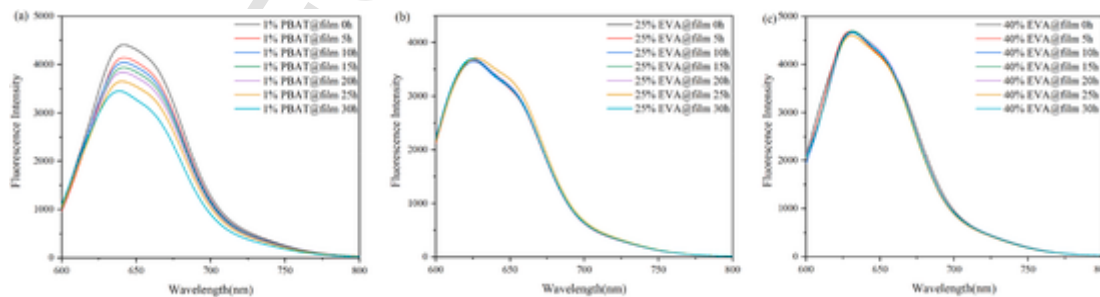


Fig. 8. The fluorescence emission spectra of (a) 1%PBAT@film, (b) 25%EVA@film and (c) 40%EVA@film of PDI-1 at different irradiation time.

40%EVA@film were recorded at 85 °C and 85% humidity for different time. After irradiation for 30h, the fluorescence intensity decreases only slightly. It shows that PDI-1 has excellent temperature and humidity resistance in 25%EVA and 40%EVA matrix (Fig. 9).

3.6. UV-visible transmittance analysis

Transmittance is an important characteristic of light conversion film. Taking three PDI-1 doped films as an example, and the corresponding blank films are used as reference, by integrating the area of the transmittance curve (Fig. 10), the transmittance of different bands are summarized in Tables S6–8. The results indicate that only less than 37% ultraviolet light (200–400 nm) and 26% yellow-green light

(500–600 nm) can penetrate through 25%EVA@film and 40%EVA@film, suggesting highly efficient shielding property to ultraviolet light and yellow-green light. More importantly, the red-orange light (600–700 nm) transmittance remains at ca. 90–93% for 25%EVA@film and 40%EVA@film, moreover, no obvious decline can be observed for 700–800 nm transmittance compared to their blank film, which indicate that doping with light conversion agents only faintly affect the visible light transmittance of the EVA film. After irradiation for different time, the transmittance of 25% EVA and 40% EVA does not fluctuate much. Compared with 25%EVA@film and 40%EVA@film, 1%PBAT@film show lower transmittance at 600–700 nm and 700–800 nm, which may be attributed to the poor compatibility between the PDI-1 and PBAT matrix. Meanwhile, trans-

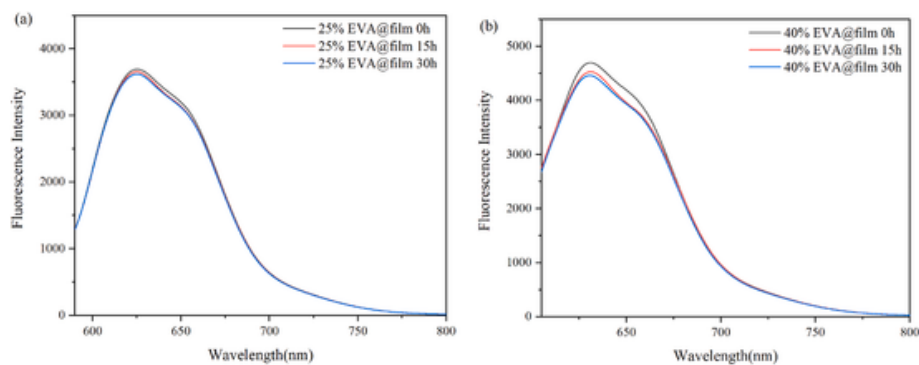


Fig. 9. The fluorescence emission spectra of 25%EVA@film and 40%EVA@film at 85 °C and 85% humidity for different time.

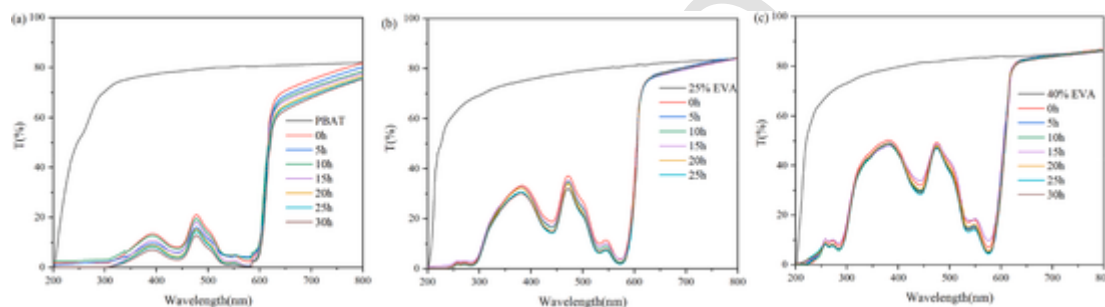


Fig. 10. UV-visible transmission spectra of 1%PBAT@film (PDI-1), 25%EVA@film, 40%EVA@film and their blank films after different irradiation time.

mittance at 200–800 nm decrease to some extent for 1%PBAT@film, indicating poor photostability for PBAT than 25%EVA and 40%EVA.

4. Conclusion

In short, three imide-substituted PDI derivatives were designed and synthesized, and their structures were characterized and confirmed by H NMR, C NMR, X-ray single crystal diffraction and HR-MS. Based on UV-vis absorption and emission spectra, the PDI derivatives exhibit obvious solvatochromism, and AIE-activity test indicates propeller-like TPE/TBM units on imide position cannot inhibit ACQ effect of PDI-2 and PDI-3. Viscosity experiment, theoretical calculation and crystal analysis show that TICT effect leads to deteriorated fluorescence for PDI-2 in solution and aggregated state, while ACQ effect of PDI-1 and PDI-3 should be attributed to intramolecular rotation and vibration of C-C, C-O and C-N bonds. The light conversion quality showed that PDI-1 has the best yellow-green light conversion properties, whose spectral composition and PFD increased up to 34% and 65% compared with that of blank film at 600–700 nm in 1%PBAT@film. The intensified UV radiation show 25%EVA@film and 40%EVA@film compared with 1%PBAT@film have significantly enhanced photostability, and their emission intensities hardly attenuated after UV radiation of 30 h, which illustrate 25% and 40% EVA with dense intermolecular hydrogen bonds are excellent light conversion film materials.

Author contribution statement

This paper is completed under the guidance of Professor Yongtao Wang, and theoretical calculation are provided by Professor Lei Ma.

Declaration of competing interest

The authors declare that they have no known competing financial interests or personal relationships that could have appeared to influence the work reported in this paper.

Data availability

Data will be made available on request.

Acknowledgements

This work was supported by the Guangxi Natural Science Foundation (Grant No. 2020GXNSFAA159147), the National Natural Science Foundation of China (Grant No. 21766030 and 21566034) and the Guilin University of Technology Research Fund (Grant No. GUTQD-JJ2019038 and GUTQDJJ2018052).

Appendix A. Supplementary data

Supplementary data to this article can be found online at <https://doi.org/10.1016/j.dyepig.2022.110948>.

References

- [1] Kume A, Akitsu T, Nasahara K.N. Leaf color is fine-tuned on the solar spectra to avoid strand direct solar radiation. *J Plant Res* 2016;129:615–24.
- [2] Kume A. Importance of the green color, absorption gradient, and spectral absorption of chloroplasts for the radiative energy balance of leaves. *J Plant Res* 2017;130:501–14.
- [3] Engelen-Eigles G, Holden G, Cohen J.D, Gardner G. The effect of temperature, photoperiod, and light quality on gluconasturtiin concentration in watercress (*Nasturtium officinale* R. Br) *J Agric Food Chem* 2006;54:328–34.
- [4] Liu D, Wang Z. Novel polyaryletherketones bearing pendant carboxyl groups and their rare earth complexes, Part I: synthesis and characterization. *Polymer* 2008;49:4960–7.
- [5] Oxley D.S, Walters R.W, Copenhafer J.E, Meyer T.Y, Petoud S, Edenborn H.M. Mono-and terfluorene oligomers as versatile sensitizers for the luminescent Eu^{3+} cation. *Inorg Chem* 2009;48:6332–4.
- [6] Wang Y, Yu Y, Liu W, Ren L, Ge G. Exploration of highly efficient blue-violet light conversion agents for an agricultural film based on structure optimization of triphenylacrylonitrile. *J Agric Food Chem* 2018;66:13295–302.
- [7] Ezati P, Rhim J.-W. Pectin/carbon quantum dots fluorescent film with ultraviolet blocking property through light conversion. *Colloid Surf. B-Biointerfaces* 2022; 112804.
- [8] Zhu Y, Ge M. Study on the energy transfer efficiency from $\text{SrAl}_2\text{O}_4: \text{Eu}^{2+}, \text{Dy}^{3+}$ to light conversion agent of red-emitting phosphor: $\text{SrAl}_2\text{O}_4: \text{Eu}^{2+}, \text{Dy}^{3+}$ /light conversion agent. *Mater Lett* 2016;182:173–6.

- [9] Liu Y, Gui Z, Liu J. Research progress of light wavelength conversion materials and their applications in functional agricultural films. *Polymers* 2022;14:851.
- [10] Jiang Y, Yan C, Zhang H, Wu M, Zheng S, Zhang Y, et al. Biodegradable poly(lactide)/rare earth complexes in light conversion agricultural films. *Coatings* 2021;11:139.
- [11] Wang D, Yu Y, Ai X, Pan H, Zhang H, Dong L. Poly(lactide)/poly (butylene adipate-co-terephthalate)/rare earth complexes as biodegradable light conversion agricultural films. *Polym Adv Technol* 2019;30:203–11.
- [12] Wang X, Qiu Z, Li Y, Mi Q, Zhou W, Ai S, et al. Core-shell structured CaS:Eu²⁺@CaZnOS via inward erosion growth to realize a super stable chalcogenide red phosphor. *J Mater Chem C* 2019;7:5931–6.
- [13] Hwang T.G, Kim G.-Y, Han J.-I, Kim S, Kim J.P. Enhancement of lipid productivity of *Chlorella sp.* using light-converting red fluorescent films based on aggregation-induced emission. *ACS Sustainable Chem Eng* 2020;8:15888–97.
- [14] Yang J, Cai Y, Zhou Y, Zhang C, Liang P, Zhao B, et al. Highly effective thieno [2,3-b] indole-diketopyrrolopyrrole near-infrared photosensitizer for photodynamic/photothermal dual mode therapy. *Dyes Pigments* 2017;147:270–82.
- [15] Zong L, Gong Y, Yu Y, Xie Y, Xie G, Peng Q, et al. New perylene diimide derivatives: stable red emission, adjustable property from ACQ to AIE, and good device performance with an EQE value of 4.93. *Sci Bull* 2018;63:108–16.
- [16] Alloa E, Grande V, Dilmurat R, Beljonne D, Würthner F, Hayes S.C. Resonance Raman study of the J-type aggregation process of a water soluble perylene bisimide. *Phys Chem Chem Phys* 2019;21:18300–9.
- [17] Kim W.S, Yoon H.I, Lee J.M, Hwang T.G, Kim H.M, Lee H.K, et al. Substituents effects on properties of perylene dyes for spectrum conversion film. *Dyes Pigments* 2022;110845.
- [18] Hwang T.G, Kim G.-Y, Han J.-I, Kim S, Kim J.P. Enhancement of lipid productivity of *Chlorella sp.* using light-converting red fluorescent films based on aggregation-induced emission. *ACS Sustainable Chem Eng* 2020;8:15888–97.
- [19] Zhao Q, Zhang S, Liu Y, Mei J, Chen S, Lu P, et al. Tetraphenylethynyl-modified perylene bisimide: aggregation-induced red emission, electrochemical properties and ordered microstructures. *J Mater Chem* 2012;22:7387–94.
- [20] Zong L, Zhang H, Li Y, Gong Y, Li D, Wang J, et al. Tunable aggregation-induced emission nanoparticles by varying isolation groups in perylene diimide derivatives and application in three-photon fluorescence bioimaging. *ACS Nano* 2018;12:9532–40.
- [21] Hwang T.G, Kim G.-Y, Han J.-I, Park J.M, Kim J.P. Highly efficient light-converting films based on diketopyrrolopyrrole with deep-red aggregation-induced emission for enhancing the lipid productivity of *Chlorella sp.* *Sustain Energy Fuels* 2021;5:5205–15.
- [22] Scheinhardt B, Trzaskowski J, Baier M.C, Stempfle B, Oppermann A, Wöll D, et al. Anisotropic polyethylene nanocrystals labeled with a single fluorescent dye molecule: toward monitoring of nanoparticle orientation. *Macromolecules* 2013;46:7902–10.
- [23] Yu Y, Wang Y, Liu W, Jia X, Ma L, Ren L, et al. Exploration of highly efficient light conversion agents for agricultural film based on the bay-substituted perylene diimides derivatives. *Dyes Pigments* 2018;159:483–90.
- [24] Ren Y, Chen Z, Du H, Fang L, Zhang X. Preparation and evaluation of modified ethylene-vinyl acetate copolymer as pour point depressant and flow improver for Jiangnan crude oil. *Ind Eng Chem Res* 2017;56:11161–6.
- [25] Xue X, Tian L, Hong S, Zhang S, Wu Y. Effects of composition and sequence of ethylene-vinyl acetate copolymers on their alcoholysis and oxygen barrier property of alcoholized copolymers. *Ind Eng Chem Res* 2019;58:4125–36.
- [26] Sadrai M, Hadel L, Sauers R.R, Husain S, Krogh-Jespersen K, Westbrook J.D, et al. Lasing action in a family of perylene derivatives: singlet absorption and emission spectra, triplet absorption and oxygen quenching constants, and molecular mechanics and semiempirical molecular orbital calculations. *J Phys Chem A* 1992;96:7988–96.
- [27] Neese F, Wennmohs F, Becker U, Riplinger C. The ORCA quantum chemistry program package. *J Chem Phys* 2020;152:224108.
- [28] Lu T, Chen F. Multiwfn: a multifunctional wavefunction analyzer. *J Comput Chem* 2012;33:580–92.
- [29] Humphrey W, Dalke A, Schulten K. VMD: visual molecular dynamics. *J Mol Graph* 1996;14:33–8.
- [30] Tylecz J.-B, Bastogne T, Bourguignon A, Frochet C, Barberi-Heyob M. Realtime tracking of the photobleaching trajectory during photodynamic therapy. *IEEE Trans Biomed Eng* 2016;64:1742–9.
- [31] Kalies S, Kuetemeyer K, Heisterkamp A. Mechanisms of high-order photobleaching and its relationship to intracellular ablation. *Biomed Opt Express* 2011;2:805–16.
- [32] Ou H, Dai S, Liu R, Ding D. Manipulating the intramolecular motion of AIEgens for boosted biomedical applications. *Sci China Chem* 2019;62:929–32.
- [33] Nassar S.J.M, Wills C, Harriman A. Inhibition of the photobleaching of methylene blue by association with urea. *ChemPhotoChem* 2019;3:1042–9.